The Astrophysical Journal Supplement Series, 203:14 (11pp), 2012 November doi:10.1088/0067-0049/203/1/14

INFRARED SPECTROSCOPY OF NEARBY RADIO ACTIVE ELLIPTICAL GALAXIES

Jeremy Mould[1,2,9], Tristan Reynolds[3], Tony Readhead[4], David Floyd[5], Buell Jannuzi[6], Garret Cotter[7], Laura Ferrarese[8], Keith Matthews[4], David Atlee[6], and Michael Brown[5]
[1] Centre for Astrophysics and Supercomputing Swinburne University, Hawthorn, Vic 3122, Australia; jmould@swin.edu.au
[2] ARC Centre of Excellence for All-sky Astrophysics (CAASTRO)
[3] School of Physics, University of Melbourne, Melbourne, Vic 3100, Australia
[4] Palomar Observatory, California Institute of Technology 249-17, Pasadena, CA 91125
[5] School of Physics, Monash University, Clayton, Vic 3800, Australia
[6] Steward Observatory, University of Arizona (formerly at NOAO), Tucson, AZ 85719
[7] Department of Physics, University of Oxford, Denys, Oxford, Keble Road, OX13RH, UK
[8] Herzberg Institute of Astrophysics Herzberg, Saanich Road, Victoria V8X4M6, Canada
Received 2012 June 6; accepted 2012 September 26; published 2012 November 1

ABSTRACT

In preparation for a study of their circumnuclear gas we have surveyed 60% of a complete sample of elliptical galaxies within 75 Mpc that are radio sources. Some 20% of our nuclear spectra have infrared emission lines, mostly Paschen lines, Brackett γ, and [Fe II]. We consider the influence of radio power and black hole mass in relation to the spectra. Access to the spectra is provided here as a community resource.

Key words: galaxies: elliptical and lenticular, cD – galaxies: nuclei – infrared: general – radio continuum: galaxies

1. INTRODUCTION

Astrophysicists have striven to learn the detailed physics of active galactic nuclei (AGNs) since black holes (BHs) were first posited as the energy source (Lynden-Bell & Rees 1971). Landmarks were the dusty torus model (Mayes et al. 1985) and the unified scheme of AGNs, which realized the implications of this geometry (Antonucci et al. 1987) from the observer's standpoint. With the advent of laser guide star adaptive optics on 10 m class telescopes, the opportunity now exists to image the circumnuclear gas in nearby active galaxies and, with the aid of detailed modeling, to understand the physics of the central 10–20 lt-yr of these powerful engines. The purpose of the project our small team has recently commenced is to study a complete sample of galaxies that are radio sources within 40 Mpc. Our work focuses first on the elliptical galaxies, as these are the simplest in terms of stellar population and gas and dust content. We emphasize nearby galaxies, as at 20 Mpc the diffraction-limited resolution of the OSIRIS instrument of the Keck Observatory is 3.2 pc, which is appropriate for disk gas heated by AGNs.[10] Central BHs are now believed to be basic constituents of most, if not all, massive galaxies (Magorrian et al. 1998; Kormendy 2004). That BH growth is linked with galaxy formation was realized because of the correlation of BH mass with the properties of the host galaxy (Kormendy 1993; Kormendy & Richstone 1995; Magorrian et al. 1998; Gebhardt et al. 2000; Ferrarese & Merritt 2000; Barth et al. 2005; Greene & Ho 2006), although alternative explanations have been put forth (Jahnke & Maccio 2010).

The deviation of the galaxy mass function from the strict power law describing dark matter halo masses provides an additional and independent argument in favor of feedback (e.g., Hopkins et al. 2008). The feedback is also relevant to the cooling flow problem, particularly with respect to radio AGNs (e.g., Bower et al. 2006; Best et al. 2006). Studies have shown that ~30% of the most massive galaxies are radio continuum sources (e.g., Fabbiano et al. 1989; Sadler et al. 1989). As a direct manifestation of accretion, and therefore BH growth, AGNs and the consequences of their energy feedback have figured prominently in most current ideas of structure formation (e.g., Granato et al. 2004; Springel et al. 2005; Hopkins & Hernquist 2006). Awareness of the importance of BHs has engendered broad interest in the study of the AGN phenomenon itself.

This paper focuses on nuclear activity in nearby galaxies. By selection, most of the objects occupy the faintest end of the AGN luminosity function and have low-accretion rates. Although energetically less impressive, low-luminosity AGNs deserve scrutiny. By virtue of proposed reasons such as duty cycle (Greene & Ho 2007) or high/low-accretion states (see, e.g., Hardcastle et al. 2006), most AGNs are found in a low-luminosity state. Brown et al. (2011) argue that all massive early-type galaxies are radio sources, mostly powered by AGNs (Slee et al. 1994; Ho 1999). The advent of new telescopes and new analysis techniques yield fresh insights into this problem.

The aims of our project are (1) to image nearby ellipticals that are radio sources in 1–2 μm emission lines, (2) to deduce the kinematics of the gas in these lines, (3) to model the density and temperature of the gas, (4) to deduce the mass of the nuclear BH and the star formation rate (SFR) in the central 10 pc, (5) to measure gas inflow and outflow rates in non-equilibrium regions of the central structure, and (6) to summarize these results over the 40 Mpc complete sample of ellipticals, noting correlations with mass, radio power, SFR, emission-line strength, and X-ray power.

In this paper, we present the first half of a survey of infrared emission lines carried out at Palomar Observatory and Kitt Peak National Observatory. A number of the galaxies show lines of [Fe II], which will be followed up with 8 m class telescopes to accomplish the first goal of our project. Circumnuclear SFRs are presented for those with Brackett γ in emission.

2. OBSERVATIONS

Brown et al. (2011) have compiled a complete sample to $K = 9$ of 396 elliptical galaxies with declination $> -40°$. The

[9] Visiting Astronomer, Kitt Peak National Observatory, National Optical Astronomy Observatory, which is operated by the Association of Universities for Research in Astronomy (AURA) under cooperative agreement with the National Science Foundation.
[10] Our sample mean is actually 40 Mpc, where the OSIRIS resolution is 6.4 pc.

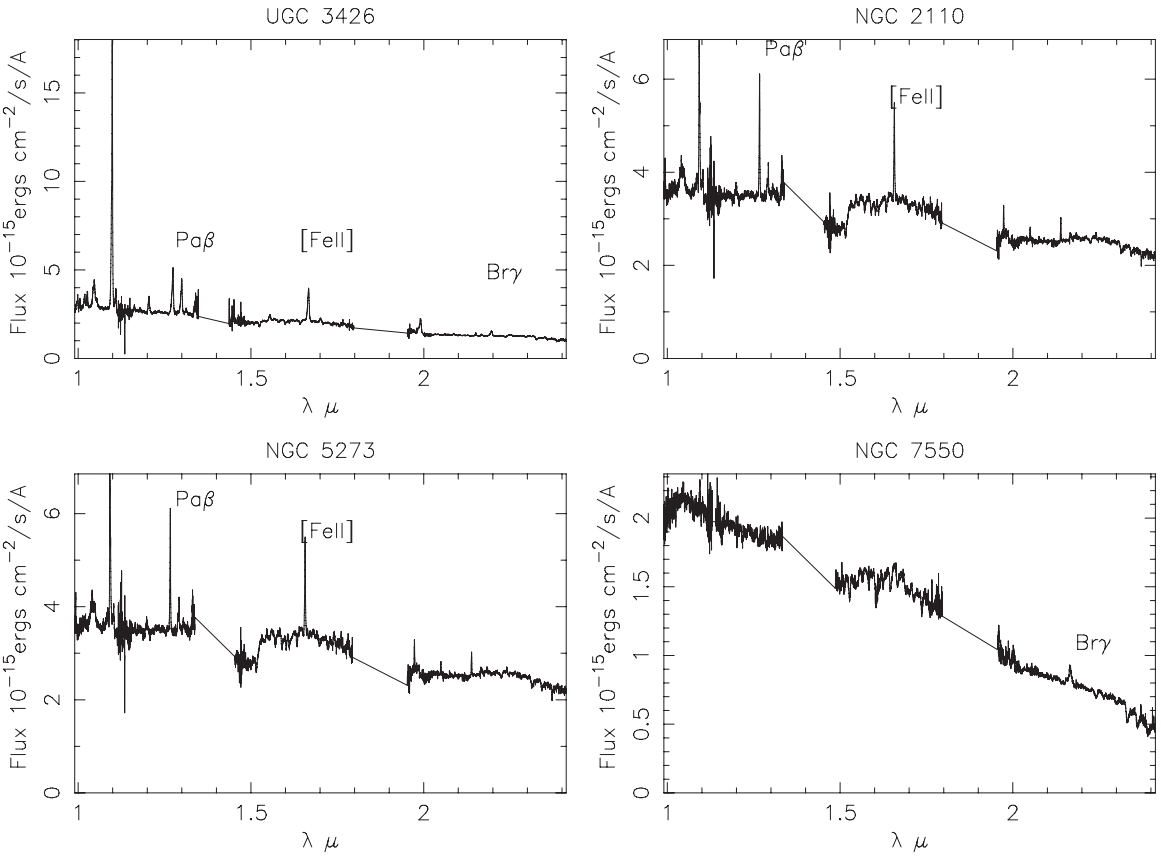

Figure 1. Palomar Triplespec spectra (1″ aperture) of three of the strongest emission-line galaxies encountered in the sample so far. [Fe II] is the strong line at 1.64 μm. Pβ is at 1.28 and Brγ at 2.18 μm. NGC 7550 has Brγ in emission, indicating a high star formation rate.

Table 1
Runs

No.	Telescope	Spectrograph	Dates	Resolution	Slit	Wavelength Range
1	Hale 5 m Palomar	Triplespec	2011 Sep 14–15	2600	1″ 4 pixels	1.0–2.4 μm
2	Mayall 4 m KPNO	Flamingos	2011 Nov 6–11	1000	1″ 3 pixels	0.9–1.8 μm
3	Hale 5 m Palomar	Triplespec	2012 Jan 2	2600	1″	1.0–2.4 μm
4	Mayall 4 m KPNO	Flamingos	2012 Feb 4–9	1000	1″	0.9–1.8 μm
5	Hale 5 m Palomar	Triplespec	2012 May 29–30	2600	1″	1.0–2.4 μm

Notes. The following radio active early-type galaxies have Palomar Triplespec spectra from J. Woo et al. (2012, in preparation): NGC 3245, 3607, 3608, 4261, 4291, 4374, 4459, 4473, 4486, 4564, 4596, 4649, 4697, 4742, 6251, and 7052. None of these galaxies have emission lines in the *H* band. The Triplespec detector format is 2048 × 1024; the Flamingos detector is 2048^2 pixels.

231 detected radio sources[11] among them are the basic sample for this paper. For diffraction-limited imaging of the centers of these galaxies with the Keck and Gemini Observatories, we have begun to observe the subsample with 1.4 GHz radio power $>10^{21}$ W Hz^{-1} and declination $>-36^{\circ}$ with the instrumentation listed in Table 1. Sample near-infrared spectra are shown in Figures 1–5 in which no redshift correction has been applied. Currently, 20% of the galaxies observed are showing emission lines of [Fe II] and/or Brγ, suitable for follow-up with Keck OSIRIS and Gemini North NIFS integral field unit (IFU) spectrographs.[12] Our five runs (Table 1) with infrared slit spectrographs have netted nuclear spectra of 136 galaxies from the basic sample. This is sufficient to understand the statistics of circumnuclear properties in current epoch ellipticals. Areas of notable incompleteness are the greater Virgo cluster area and the southern hemisphere. Black hole masses in Table 4 are based on the *K*-band magnitude, following Graham (2007).

At both telescopes all galaxies were observed in two slit positions, A and B, separated by 20″, in an ABBA sequence of 4–5 minute exposures. Following the object sequence, an eighth magnitude A0V star was observed within an air mass of 0.1 of the object for telluric correction. This was also used for spectrophotometric calibration, which employed Vega model

[11] Galaxies for which upper limits were given in Brown's data table were omitted.

[12] For all but the faintest nuclei, on-axis guiding is possible.

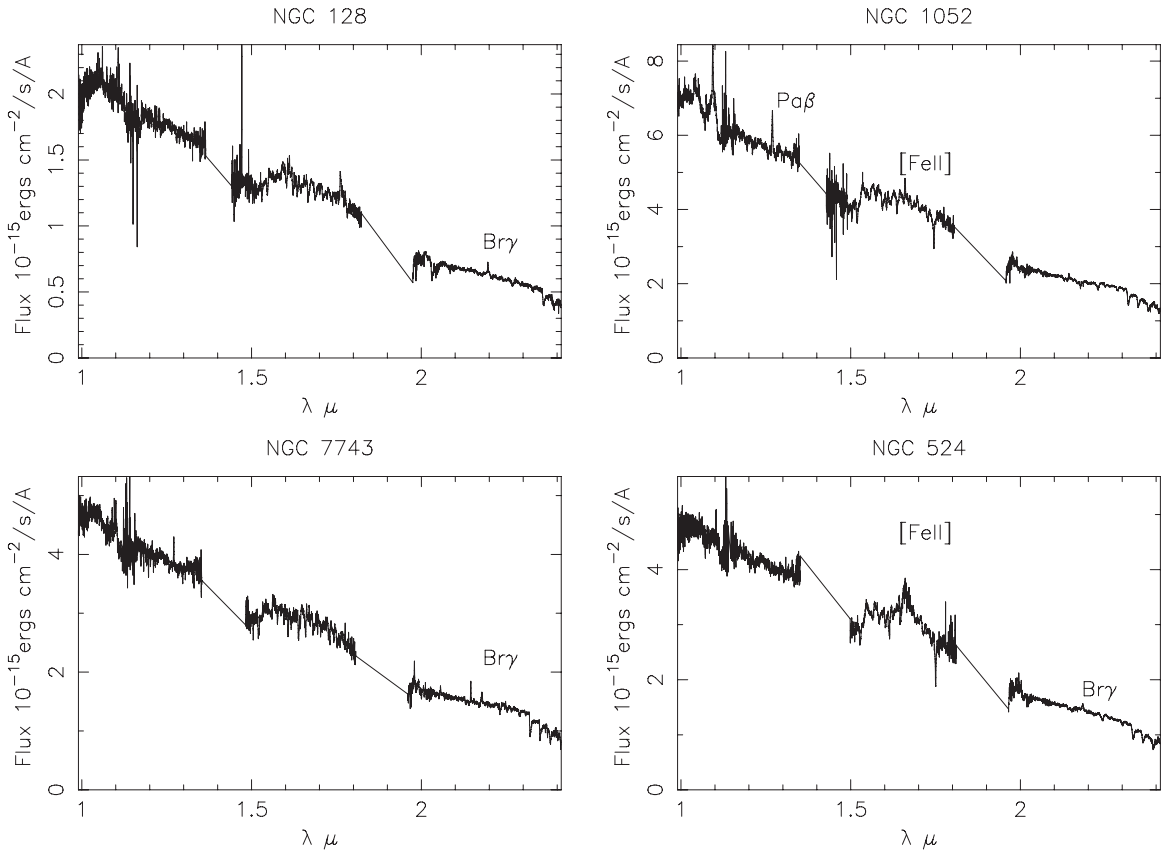

Figure 2. Palomar Triplespec spectra of emission-line nuclei. The absorption features beyond 2.3μ are CO band heads from the stellar nucleus.

fluxes for zeroth visual magnitude. For wavelength calibration an argon lamp was used at Kitt Peak and telluric OH lines were used at Palomar.

The galaxies with emission lines in these near-infrared spectra are listed in Table 2; those without are in Table 3, which also gives the signal-to-noise ratio of the Kitt Peak spectra at 1.01μ and Palomar spectra at 1.04μ.

3. DATA REDUCTION

The data sets from each observatory required different data reduction packages. The Kitt Peak National Observatory data was reduced using IRAF and the reduction of the Palomar Observatory data was done using Spextool v4.0 beta. (Cushing et al. 2004).

The first step in the reduction of the Kitt Peak data was the creation of the flat field and dark images. The flat field was created by subtracting the flat lamps-off image from the flat lamps-on image. The first and second nights' data had separate flat-field images. The third night's data set did not contain flat-field images, so the flat-field image created for night 2 was also used for night 3 objects.

For the standard stars, from the observation files the dark image was subtracted and then the flat-field image was divided out. The spectrum was then extracted using the task "apall" in IRAF. As the observation files for the galaxies were taken as ABBA, the galaxy spectra were extracted by creating images for A–B and B–A files, which were then divided by the flat-field image. The flat fielded A–B and B–A images were then rotated and cropped before running "apall" on each image.

The axes for the spectra were initially in terms of pixels and had to be wavelength calibrated using an argon arc spectrum. This was achieved by picking five prominent peaks in the arc spectrum and identifying the pixel value corresponding to the wavelength of each peak. These five values were then used to interpolate along the entire spectrum.

To create the flat-field image used with the Palomar data, IRAF was first used to form a set of flat-field images by subtracting the individual flat lamp-off images from the flat lamp-on images. The flat-field images created with IRAF were then used in the program "xspextool" in Spextool to create the master flat field. The wavelength calibration was created in "xspextool" using any four galaxy images. The spectra for the galaxies and standard stars were extracted in "xspextool" for A–B and B–A image sets using the master flat-field image and the wavelength calibration.

The individual extracted spectra for each galaxy and standard star were then combined using "xcombspec" by selecting all images of each object and scaling all orders with respect to the spectrum with the greatest magnitude in the order 3 spectrum.

Telluric correction was carried out on the combined spectra for each galaxy using the combined standard star spectra with a similar air mass to the galaxy using the Spextool program "xtellcor". The hydrogen absorption lines in the standard star spectrum were rescaled for all orders and the telluric spectrum was constructed. The four orders (3,4,5,6) of the telluric-corrected galaxy spectra were merged using "xmergeorders" to give a single spectrum.

Spectra are provided for readers desiring access to them.[13] Cesetti et al. (2009) show spectra of NGC 4649, NGC 4697,

[13] https://sites.google.com/site/radioactivegalaxies/

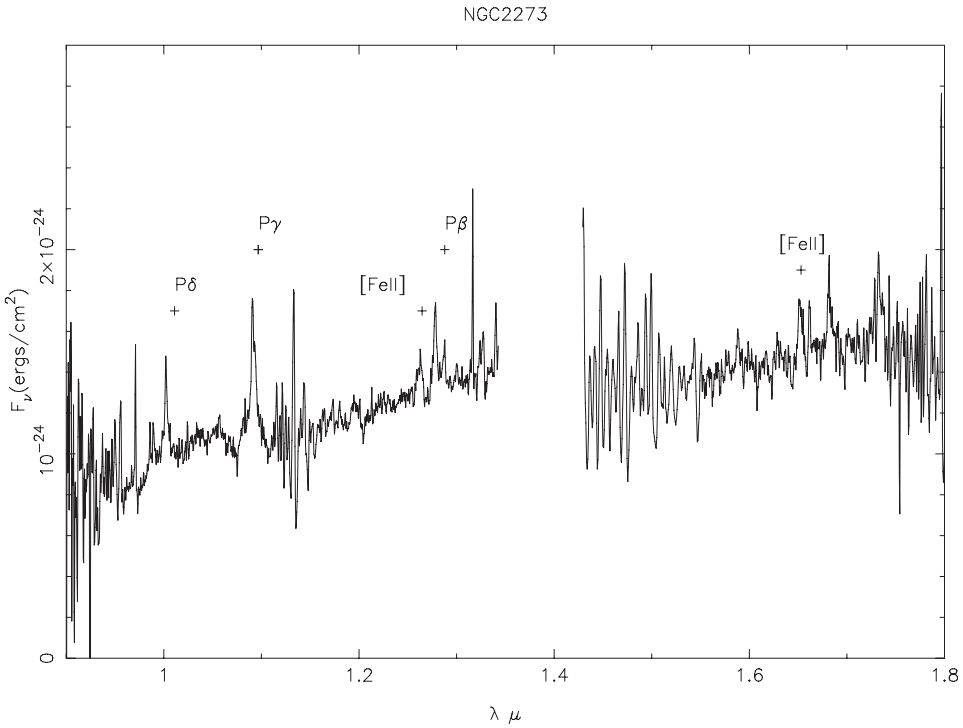

Figure 3. Flamingos spectrum of NGC 2273. The Paschen emission lines, such as Pγ 1.09μ, may thus be exaggerated. Three-point boxcar smoothing has been applied.

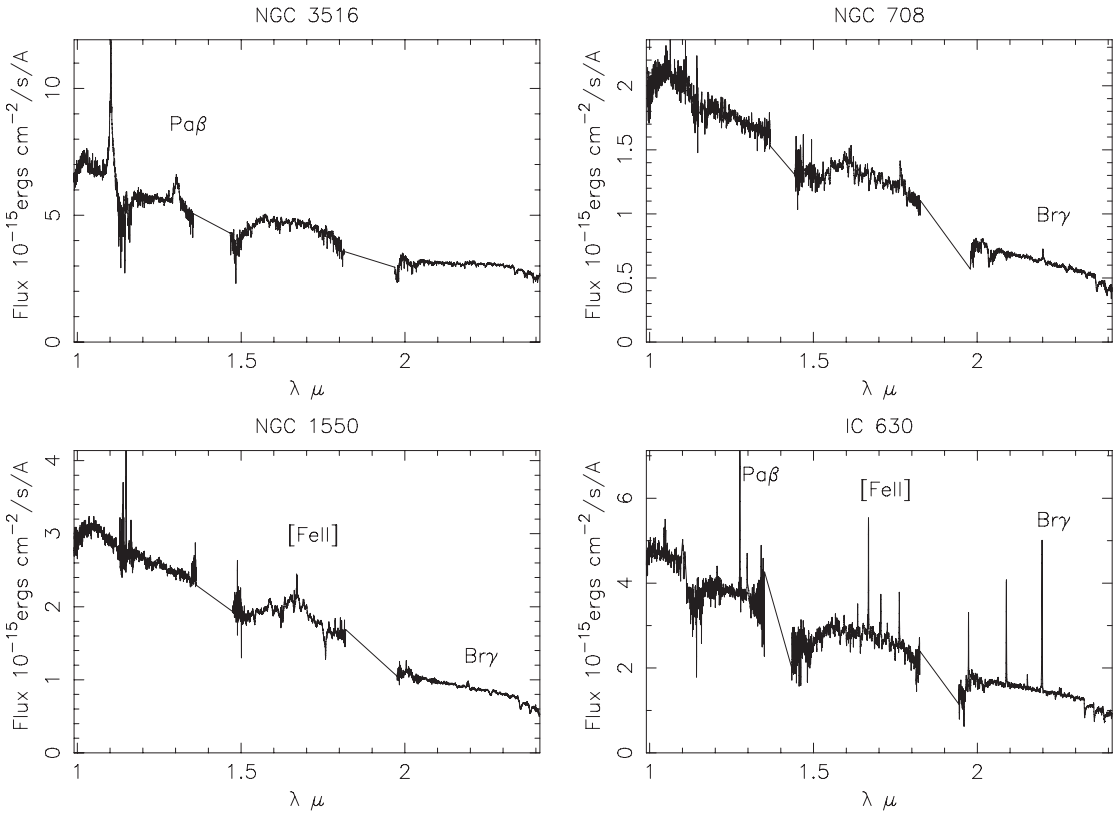

Figure 4. Further Palomar spectra of emission-line nuclei.

IC 4296, NGC 4564, NGC 5077, and NGC 5576. Riffel et al. (2006) show a spectrum of NGC 2110.

4. DISCUSSION

We compare the radio power of our emission-line galaxies with that of the full 397 galaxy Brown et al. sample in Figure 6. Infrared emission-line nuclei have six times stronger radio emission than average at a given *K*-band magnitude (or stellar mass). This does not stand out in the figure, but is a 4σ effect, based on the line in Figure 6 and the scatter in the relation. Both radio and infrared quantities here are from the data table of Brown et al. The whole-sample correlation may be expected on general scaling grounds. A larger galaxy hosts a larger BH,

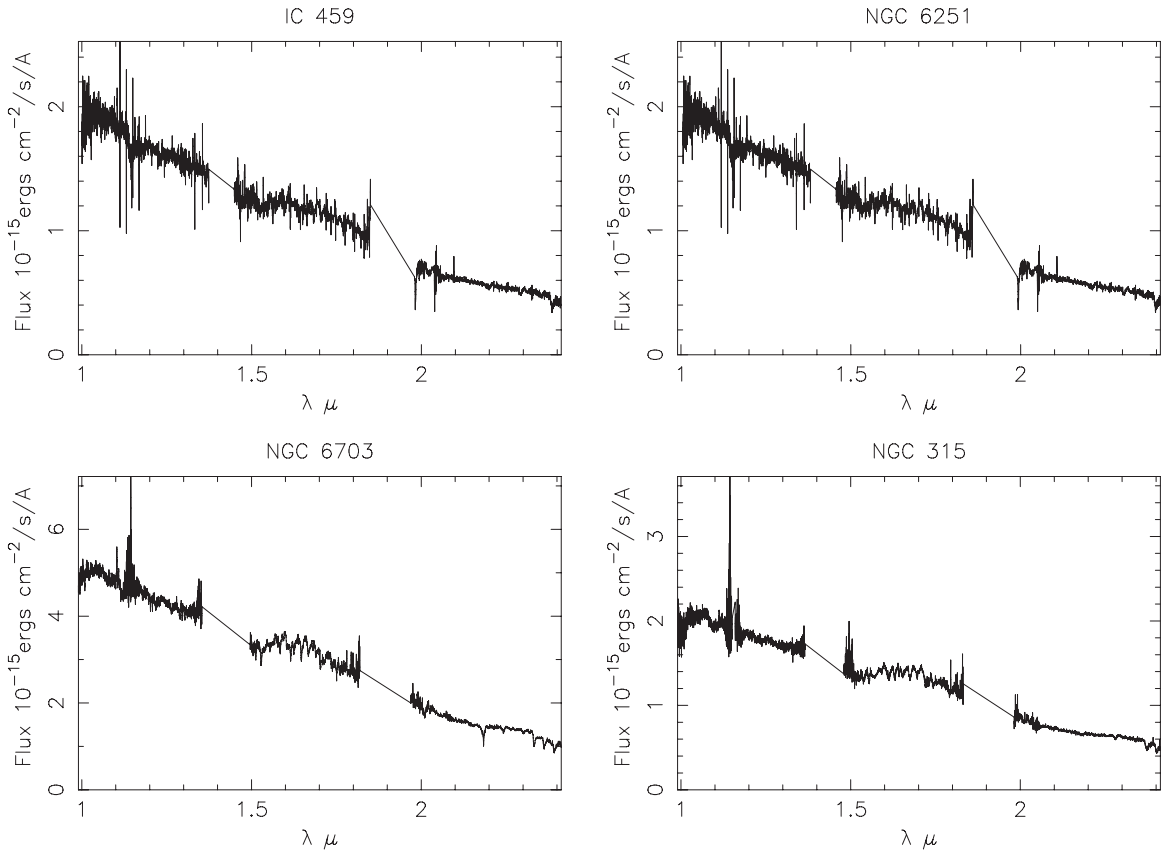

Figure 5. Palomar spectra of absorption-line nuclei. CO band heads are seen at the red end of the 2μ window. NG 6703 has Brγ in absorption.

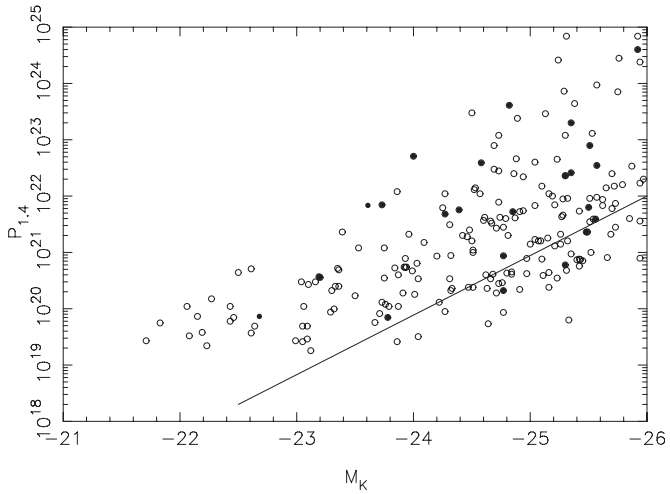

Figure 6. Radio power (W Hz^{-1}) at 1.4 GHz vs. absolute K magnitude. The data are from Brown et al. (2011). Galaxies whose radio powers are upper limits are not distinguished. Emission-line nuclei are denoted by solid symbols. The line is from the original reference and is the median radio power as a function of K-band luminosity for all ellipticals (including those not detected by NVSS). As this sample only includes radio sources, it is automatically biased toward higher radio powers and is systematically above the line.

which in turn is responsible for more radio power. Indeed, Ho (2008) shows a strong correlation between radio loudness and X-ray luminosity divided by Eddington ratio. However, if our infrared emission-line galaxies stand out, it may be because the BH in these cases is currently being fed by the circumnuclear disk.

We also examined the thermal infrared fluxes of the emission-line galaxies. Only UGC 3426 and NGC 3516 had mid-infrared excesses in the *AKARI* Point Source Catalog (Murakami et al. 2007): The former has a $9\mu/2.2\mu$ flux ratio of 1.7 and the latter 1.0. The infrared flux of UGC 3426 rises a further factor of six at 18μ. In general, the *IRAS* fluxes of our near-infrared emission-line galaxies do not correlate well with the SFR in Table 2 (Figure 7).

The infrared emission-line spectra in Table 2 are not all clones of one another. We compare the Brγ profiles of NGC 2787 and IC 630 in Figure 8. The former has a broad rounded profile, FWHM 750 km s^{-1}. The latter has a sharp profile, FWHM 200 km s^{-1}. The former is a LINER (Balzano 1983) and the latter is a starburst nucleus in the Veron-Cetty & Veron (2006) catalog. Both are morphologically classified S0. These differences are a strong motivation to explore the spatial structure of the emitting gas at 10 m class diffraction limited resolution.

In Figure 9, we show the relation between BH mass and SFR. The latter is calculated from Brγ (Kennicutt 1998). SFR uncertainties were calculated from the Brγ uncertainties in Table 2. We draw the uncertainty in the BH mass from Table 4 where both the (K, $M_{\rm BH}$) and (σ, $M_{\rm BH}$) relations are employed and the galaxies have secondary distance indicators. It is largely a scatter plot, although the sample is modest, and there is a hint of a correlation in the galaxy scaling sense. If the BH formation process were steady in solar masses/year, one might expect a correlation. If the process is sporadic, dependent, for example, on fueling events or circumnuclear disk instability, a correlation would easily be masked. Monitoring Brγ over time or high-resolution analysis of any disk could shed light on this.

Table 2
Emission Line Nuclei

NAME	R.A. (2000)	Decl.	Run	Brγ Flux (erg cm^{-2} s^{-1})	SFR ($M_\odot$ yr^{-1})	Remarks	$P_{1.4}$ (W Hz^{-1})	Redshift
NGC 128	00:29:15	+02:51:51	1	1.11 ± 0.04E−15	0.38	1.74μ unident.	6.0E+20	0.014
NGC 524	01:24:48	+09:32:19	1	1.85 ± 0.06E−15	0.18	very broad 1.6μ	2.1E+20	0.008
NGC 547	01:26:01	−01:20:42	1	3.97 ± 0.04E−16	0.18		4.0E+24	0.018
NGC 665	01:44:56	+10:25:23	1	6.92 ± 0.03E−16	0.38		6.3E+21	0.018
NGC 708	01:52:46	+36:09:06	1	9.1 ± 0.9E−16	0.37		3.5E+22	0.016
NGC 1052	02:41:05	−08:15:21	1			1.26, 1.64μ [Fe II]	5.1E+22	0.005
NGC 1521	04:08:19	−21:03:07	3	4.62 ± 0.05E−15	1.5		2.3E+21	0.014
NGC 1550	04:19:38	+02:24:35	1	1.27 ± 0.03E−15	0.31		5.3E+21	0.012
NGC 2110	05:52:11	−07:27:22	1				3.9E+22	0.008
NGC 2128	06:04:34	+57:37:40	1	1.7 ± 0.1E−15	0.31		5.7E+21	0.010
NGC 2273	06:50:08	+60:50:45	4			[Fe II] lines	6.8E+21	0.006
UGC3426	06:15:36	+71:02:15	1	1.2 ± 0.02E−13	37.2		4.1E+23	0.0135
NGC 2768	09:11:38	+60:02:14	1				8.7E+20	0.004
NGC 2787	09:19:18	+69:12:12	1	1.63 ± 0.05E−14	0.31		7.3E+19	0.002
NGC 2859	09:24:19	+34:30:49	1	7.7 ± 0.4E−15	0.49		7.0E+19	0.006
NGC 3065	10:01:55	+72:10:13	1	1.8 ± 0.1E−15	0.18		3.6E+20	0.007
IC630	10:38:33	−07:10:14	3	1.99 ± 0.01E−14	2.1		7.0E+21	0.007
NGC 3516	11:06:47	+72:34:07	3			Broad Pβ	4.8E+21	0.009
NGC 4111	12:07:03.1	+43:03:57	5	1.5 ± 0.1E−15	0.04	+	2.5E+20	0.003
NGC 5273	13:42:08.3	+35:39:15	5			Broad Pγ	1.1E+20	0.004
NGC 5322	13:49:15.3	+60:11:26	5	1.9 ± 0.8E−15	0.18		9.1E+21	0.006
NGC 7052	21:18:33	+26:26:49	1	2.49 ± 0.07E−15	1.03		7.9E+22	0.016
NGC 7426	22:56:03	+36:21:41	1	3.75 ± 0.09E−15	2.01		3.9E+21	0.018
NGC 7550	23:15:16	+18:57:42	1	1.77 ± 0.04E−15	0.86		2.6E+22	0.017
NGC 7618	23:19:47	+42:51:10	1	1.94 ± 0.04E−15	0.99		2.3E+22	0.017
NGC 7626	23:20:43	+08:13:01	1	1.86 ± 0.06E−15	0.43		2.0E+23	0.011
NGC 7743	23:44:21	+09:56:03	1	1.90 ± 0.07E−15	0.09		3.7E+20	0.006

Notes. The remark on broad Paschen lines applies to all four of NGC 3516, 3557, 4111, and 5273. The redshifts in Column 9 are the literature, not observed, values.

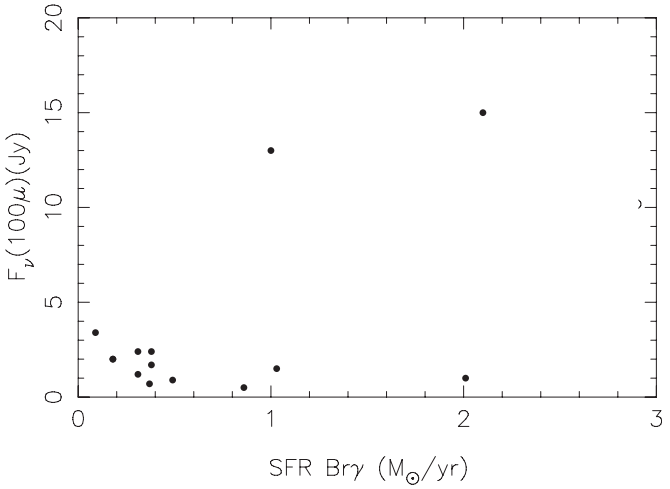

Figure 7. Comparison of the Brγ star formation rates with *IRAS* far infrared fluxes. UGC 3426 is the upper limit at 10 Jy.

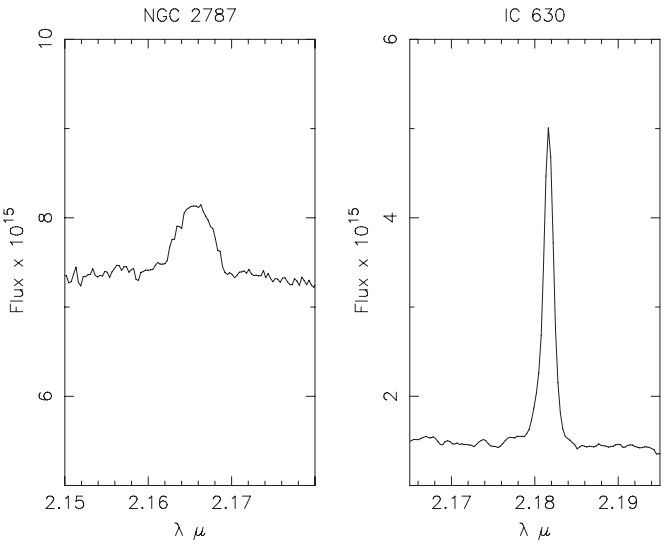

Figure 8. Comparison of the Brγ profiles of two galaxies. The spectra have not been corrected to the rest frame.

Table 3
Absorption Line Nuclei

NAME	Run	S/N	NAME	Run	S/N
NGC 16	1	93	NGC 3091	4	3
NGC 50	2	8	NGC 3100	3	
NGC 57	4	14	NGC 3158	2	23
NGC 315	1	50	NGC 3226	2	22
NGC 383	1		NGC 3245	2	24
NGC 410	1	22	NGC 3348	4	8
NGC 439	3		NGC 7454	2	10
NGC 474	1	49	NGC 3414	2	30
NGC 499	4	12	NGC 3528	4	20
NGC 533	2	2	NGC 3607	4	38
NGC 596	4	20	NGC 3619	4	26
NGC 680	4	13	NGC 3626	4	14
NGC 741	2	7	NGC 3665	4	34
NGC 883	2	7	NGC 3801	4	7
NGC 936	2	10	NGC 3872	4	17
NGC 1016	2	2	NGC 3894	4	20
NGC 1060	2	15	NGC 3957	4	11
NGC 1128	1	70	NGC 3962	4	31
NGC 1167	1	52	NGC 3986	4	14
NGC 1200	2		NGC 4008	4	5
NGC 1209	4	10	NGC 4036	4	31
NGC 1326	3	74	NGC 4125	4	31
NGC 1399	3	95	NGC 4138	4	28
NGC 1400	2		NGC 4220	4	17
NGC 1407	2	8	NGC 4589	4	22
NGC 1453	1	89	NGC 4636	4	25
NGC 1531	3	15	NGC 4778	4	8
IC359	2		NGC 4782	4	17
UGC3024	2	6	NGC 4802	4	15
NGC 1587	1	64	NGC 4825	4	19
NGC 1600	2	8	NGC 4874	4	8
NGC 1573	2	10	NGC 4984	4	28
NGC 1653	1	70	NGC 5044	4	6
NGC 1684	1	68	NGC 5077	4	16
NGC 1726	2	10	NGC 5198	4	20
NGC 2089	2	8	NGC 5444	4	23
NGC 2208	2	4	NGC 5490	4	21
NGC 2256	4	4	NGC 5532	4	9
NGC 2258	2	28	NGC 5631	4	21
NGC 2320	4	15	NGC 5838	4	16
NGC 2314	4	9	IC 459	3	26
NGC 2340	2	8	NGC 5846	1	32
NGC 2418	4	20	NGC 6251	1	53
NGC 2493	3	85	NGC 6482	1	49
NGC 2513	2	30	NGC 6703	1	67
NGC 2612	4	24	NGC 6869	2	8
UGC3789	4	15	NGC 6903	2	8
NGC 2629	3	71	NGC 7242	2	7
NGC 2685	1	47	NGC 7265	2	13
NGC 2693	3	82	NGC 7391	2	11
NGC 2749	2	23	NGC 7436	2	22
NGC 2872	3	78	NGC 7562	2	7
NGC 2911	1	19	NGC 7600	2	9
NGC 2974	4	55	NGC 7711	1	83
NGC 3078	3	103	NGC 7785	1	69
NGC 4551	5	50	NGC 5796	4	23
NGC 5813	5	54	NGC 4143	5	87
NGC 4203	5	97	NGC 4150	5	64
NGC 4278	5	83	NGC 4710	5	29
NGC 4866	5	47	NGC 5353	5	93

Table 4
BH Masses For Brown et al. (2011) Galaxies

Name	R.A.[a] (J2000)	Decl.	$m-M$[b] (mag)	Method[c]	K[d] (2MASS)	σ[e] (km s^{-1})	$M(\mathrm{BH})_K$[f] ($10^8\ M_\odot$)	$M(\mathrm{BH})_\sigma$[g] ($10^8\ M_\odot$)	Notes[h]
NGC 0016	00:09:04	+27:43:45	33.2	CV	8.78	180	3.18	0.99	
NGC 0050	00:14:44	−07:20:42	34.4	CV	8.67	264	11.77	6.40	
NGC 0057	00:15:30	+17:19:42	34.4	CV	8.68	326	11.41	17.84	
NGC 0128	00:29:15	+02:51:50	33.9	CV	8.52	215	7.90	2.36	
NGC 0315	00:57:48	+30:21:29	34.2	CV	7.95	279	18.89	8.37	
NGC 0383	01:07:24	+32:24:44	34.2	CV	8.48	279	12.10	8.37	
NGC 0410	01:10:58	+33:09:08	34.3	CV	8.38	300	14.41	11.91	
NGC 0439	01:13:47	−31:44:49	34.5	CV	8.70	221	12.65	2.70	
NGC 0474	01:20:06	+03:24:55	32.5	CV	8.55	163	2.18	0.61	
NGC 0499	01:23:11	+33:27:36	33.9	CV	8.73	266	6.94	6.64	
NGC 0524	01:24:47	+09:32:19	32.6	CV	7.16	253	8.77	5.20	
NGC 0533	01:25:31	+01:45:32	34.4	CV	8.44	279	14.92	8.37	
NGC 0547	01:26:00	−01:20:42	34.4	CV	8.49	260	13.85	5.94	
NGC 0596	01:32:51	−07:01:53	32.1	CV	7.97	152	2.40	0.44	
NGC 0665	01:44:56	+10:25:23	34.4	CV	8.88	190	9.37	1.29	
NGC 0680	01:49:47	+21:58:14	33.0	CV	8.73	212	2.70	2.20	
NGC 0708	01:52:46	+36:09:07	34.1	CV	8.57	230	9.94	3.27	
NGC 0741	01:56:20	+05:37:43	34.4	CV	8.29	291	17.40	10.27	
NGC 0883	02:19:05	−06:47:27	34.3	CV	8.89	287	8.84	9.60	
NGC 0936	02:27:37	−01:09:21	31.4	CV	6.91	189	3.34	1.26	
NGC 1016	02:38:19	+02:07:09	34.1	D_n–σ	8.58	302	10.02	12.30	
NGC 1052	02:41:04	−08:15:20	31.4	SBF	7.45	207	2.16	1.96	
NGC 1060	02:43:15	+32:25:29	34.3	D_n–σ	8.20	303	16.18	12.50	
NGC 1128	02:57:42	+06:01:29	34.9	CV	8.98	...	14.72	...	
NGC 1167	03:01:42	+35:12:20	34.2	CV	8.64	171	9.68	0.78	
NGC 1200	03:03:54	−11:59:29	33.7	CV	8.58	204	6.56	1.83	
NGC 1209	03:06:02	−15:36:40	32.8	SBF	8.32	230	3.37	3.27	
NGC 1316	03:22:41	−37:12:29	31.7	SBF	5.59	228	16.23	3.14	
NGC 1326	03:23:56	−36:27:52	31.4	TF	7.45	118	2.04	0.13	
NGC 1399	03:38:29	−35:27:02	31.6	SBF	6.31	346	7.64	23.8 5.1 ± 0.7	(3)
NGC 1400	03:39:30	−18:41:17	31.1	SBF	7.81	252	1.06	5.10	
NGC 1407	03:40:11	−18:34:48	31.1	SBF	6.70	271	3.12	7.27	
NGC 1453	03:46:27	−03:58:08	33.7	D_n–σ	8.12	328	10.38	18.38	
NGC 1521	04:08:18	−21:03:06	34.1	SBF	8.68	242	8.98	4.19	
NGC 1531	04:11:59	-32:51:03	30.6	TF	8.42	112	0.36	0.10	
IC0359	04:12:28	+27:42:06	33.8	CV	8.47	...	7.54	...	
NGC 1550	04:19:37	+02:24:35	33.6	CV	8.77	308	4.68	13.54	
UGC3024	04:22:26	+27:17:52	34.3	CV	9.25	...	6.10	...	
NGC 1587	04:30:39	+00:39:42	32.8	D_n–σ	8.51	227	2.86	3.07	
NGC 1600	04:31:39	−05:05:09	33.5	D_n–σ	8.04	334	9.41	20.07	
NGC 1573	04:35:03	+73:15:44	33.9	D_n–σ	8.55	303	7.80	12.50	
NGC 1653	04:45:47	−02:23:33	33.8	SBF	8.97	246	4.95	4.54	
NGC 1684	04:52:31	−03:06:21	33.9	CV	8.69	306	7.25	13.11	
NGC 1726	04:59:41	−07:45:19	33.0	D_n–σ	8.61	246	3.20	4.54	
NGC 2089	05:47:51	−17:36:09	33.0	CV	8.81	206	2.57	1.92	
NGC 2110	05:52:11	−07:27:22	32.6	CV	8.14	255	3.46	5.41	
NGC 2128	06:04:34	+57:37:40	33.1	CV	8.83	261	2.87	6.05	
UGC3426	06:15:36	+71:02:15	33.8	CV	8.97	283	4.65	8.97	
NGC 2208	06:22:34	+51:54:34	34.5	CV	9.04	225	9.34	2.94	
NGC 2256	06:47:13	+74:14:11	34.3	CV	8.67	221	10.73	2.70	
NGC 2258	06:47:46	+74:28:54	33.6	SBF	8.23	287	7.93	9.60	
NGC 2273	06:50:08	+60:50:44	32.3	TF	8.48	123	1.77	0.16	
NGC 2273	06:50:08	+60:50:44	32.3	TF	8.48	123	1.77	0.16	
NGC 2320	07:05:41	+50:34:51	34.5	SNIa	8.85	315	10.69	15.10	
NGC 2314	07:10:32	+75:19:36	34.0	D_n–σ	8.88	286	6.70	9.44	
IC0459	07:10:38	+50:10:37	34.5	CV	11.29	...	0.99	...	
NGC 2340	07:11:10	+50:10:28	34.7	D_n–σ	8.88	246	13.18	4.54	
UGC3789	07:19:30	+59:21:18	33.3	CV	9.51	...	1.75	...	
NGC 2418	07:36:37	+17:53:02	34.2	CV	8.95	247	7.50	4.63	
NGC 2493	08:00:23	+39:49:49	33.7	CV	8.83	249	4.94	4.82	
NGC 2513	08:02:24	+09:24:47	33.9	D_n–σ	8.74	274	6.51	7.67	
NGC 2612	08:33:50	−13:10:28	31.8	CV	8.78	...	0.83	...	
NGC 2629	08:47:15	+72:59:08	33.6	CV	8.85	298	4.37	11.53	
NGC 2685	08:55:34	+58:44:03	30.9	TF	8.35	94	0.54	0.04	
NGC 2693	08:56:59	+51:20:50	34.0	D_n–σ	8.60	349	8.27	24.84	

Table 4
(Continued)

Name	R.A.[a] (J2000)	Decl.	$m-M$[b] (mag)	Method[c]	K[d] (2MASS)	σ[e] (km s^{-1})	$M(\mathrm{BH})_K$[f] ($10^8\ M_\odot$)	$M(\mathrm{BH})_\sigma$[g] ($10^8\ M_\odot$)	Notes[h]
NGC 2749	09:05:21	+18:18:47	33.9	D_n–σ	8.93	260	5.50	5.94	
NGC 2768	09:11:37	+60:02:14	31.8	SBF	7.00	181	4.53	1.02	
NGC 2787	09:19:18	+69:12:11	29.4	SBF	7.26	194	0.35	1.43 $1.04^{+0.36}_{-0.64}$	(1)
NGC 2859	09:24:18	+34:30:48	32.0	TF	8.04	181	2.17	1.02	
NGC 2872	09:25:42	+11:25:55	33.9	D_n–σ	8.72	284	6.75	9.12	
NGC 2911	09:33:46	+10:09:07	33.3	CV	8.71	217	3.72	2.47	
NGC 2974	09:42:33	−03:41:57	31.7	SBF	6.25	238	8.51	3.87	
NGC 3078	09:58:24	−26:55:33	32.7	SBF	7.88	251	4.97	5.01	
NGC 3091	10:00:14	−19:38:10	33.6	D_n–σ	8.09	321	9.20	16.55	
NGC 3100	10:00:40	−31:39:51	32.8	CV	8.08	200	4.27	1.66	
NGC 3065	10:01:55	+72:10:13	32.5	TF	8.99	160	1.34	0.56	
NGC 3158	10:13:50	+38:45:53	34.5	D_n–σ	8.80	343	11.47	22.84	
NGC 3226	10:23:26	+19:53:53	31.9	SBF	8.57	193	1.10	1.40	
NGC 3245	10:27:18	+28:30:26	31.6	SBF	7.86	210	1.70	2.10 2.04 ±0.49	(4)
IC0630	10:38:33	−07:10:14	32.4	CV	8.65	...	1.73	...	
NGC 3348	10:47:09	+72:50:22	32.7	D_n–σ	7.96	238	4.45	3.87	
NGC 3414	10:51:16	+27:58:28	32.0	SBF	7.98	237	2.25	3.79	
NGC 3516	11:06:47	+72:34:06	33.0	TF	8.51	157	3.34	0.51	
NGC 3497	11:07:18	−19:28:17	33.5	CV	8.67	224	5.02	2.88 == NGC 3528	
NGC 3607	11:16:54	+18:03:09	31.8	SBF	6.99	224	4.74	2.88 1.33 ±0.44	(5)
NGC 3619	11:19:21	+57:45:28	32.2	TF	8.57	162	1.57	0.60	
NGC 3626	11:20:03	+18:21:26	31.5	SBF	8.16	142	1.17	0.31	
NGC 3665	11:24:43	+38:45:46	32.6	TF	7.68	184	5.11	1.11	
NGC 3801	11:40:16	+17:43:41	33.4	CV	8.88	198	3.67	1.58	
NGC 3872	11:45:49	+13:46:00	33.3	D_n–σ	8.51	260	4.75	5.94	
NGC 3894	11:48:50	+59:24:56	33.2	CV	8.56	265	4.28	6.52	
NGC 3957	11:54:01	−19:34:06	32.2	TF	8.69	...	1.36	...	
NGC 3962	11:54:40	−13:58:29	32.7	SBF	7.67	233	6.17	3.49	
NGC 3986	11:56:44	+32:01:18	33.3	CV	8.98	196	2.89	1.50	
NGC 4008	11:58:17	+28:11:32	33.4	D_n–σ	8.83	226	3.65	3.01	
NGC 4036	12:01:26	+61:53:44	31.9	TF	7.56	181	3.18	1.02	
NGC 4125	12:08:06	+65:10:26	31.9	SBF	6.86	227	5.95	3.07	
NGC 4138	12:09:29	+43:41:06	30.7	SBF	8.20	140	0.51	0.29	
NGC 4220	12:16:11	+47:52:59	31.4	TF	8.13	125	1.05	0.17	
NGC 4589	12:37:25	+74:11:30	31.7	SBF	7.76	224	2.09	2.88	
NGC 4636	12:42:49	+02:41:15	30.8	SBF	6.42	203	3.24	1.78	
NGC 4778	12:53:06	−09:12:14	33.9	CV	8.63	232	7.35	3.42 ==NGC 4759	
NGC 4782	12:54:35	−12:34:06	33.9	D_n–σ	7.75	326	16.64	17.84	
NGC 4802	12:55:49	−12:03:18	30.3	SBF	8.50	...	0.26	...	
NGC 4825	12:57:12	−13:39:52	33.9	CV	8.51	308	8.51	13.54	
NGC 4874	12:59:35	+27:57:34	35.0	GCLF	8.86	279	17.49	8.37	
NGC 4984	13:08:57	−15:30:58	31.6	TF	7.74	...	1.98	...	
NGC 5044	13:15:23	−16:23:04	32.5	SBF	7.71	242	4.56	4.19	
NGC 5077	13:19:31	−12:39:21	32.9	D_n–σ	8.22	256	4.24	5.51	
NGC 5198	13:30:11	+46:40:14	33.4	D_n–σ	8.90	196	3.49	1.50	
NGC 5444	14:03:24	+35:07:55	33.7	D_n–σ	8.84	229	5.13	3.21	
NGC 5490	14:09:57	+17:32:43	34.5	SNIa	8.92	288	10.59	9.77	
NGC 5532	14:16:52	+10:48:32	35.1	CV	8.76	294	20.22	10.80	
NGC 5631	14:26:33	+56:34:57	32.2	SBF	8.47	171	1.72	0.78	
NGC 5796	14:59:23	−16:37:25	32.9	D_n–σ	8.15	273	4.36	7.53	
NGC 5838	15:05:26	+02:05:58	32.3	TF	7.58	266	4.26	6.64	
NGC 5846	15:06:29	+01:36:20	32.0	SBF	6.93	239	6.01	3.95	
NGC 6251	16:32:31	+82:32:16	35.1	CV	9.03	325	15.63	17.57 6.0 ± 0.2	(6)
NGC 6482	17:51:48	+23:04:18	33.7	CV	8.37	308	7.82	13.54	
NGC 6703	18:47:18	+45:33:01	32.1	SBF	8.25	178	1.95	0.94	
NGC 6869	20:00:42	+66:13:39	32.5	SBF	8.71	166	1.83	0.67	
NGC 7052	21:18:33	+26:26:48	34.1	CV	8.57	284	9.20	9.12 $3.7^{+2.6}_{-1.5}$	(2)
NGC 7242	22:15:39	+37:17:55	34.5	CV	8.33	...	17.95	...	
NGC 7265	22:22:27	+36:12:35	34.2	CV	8.69	258	9.79	5.72	
NGC 7391	22:50:36	−01:32:41	34.0	D_n–σ	8.63	244	8.08	4.36	
NGC 7426	22:56:02	+36:21:40	34.3	CV	8.81	...	9.55	...	
NGC 7436	22:57:57	+26:09:00	35.0	CV	9.01	352	15.77	25.90	
NGC 7454	23:01:06	+16:23:18	31.9	SBF	8.86	114	0.86	0.11	
NGC 7454	23:01:06	+16:23:18	31.9	SBF	8.86	114	0.86	0.11	
NGC 7550	23:15:16	+18:57:40	34.2	CV	8.91	255	7.90	5.41	

Table 4
(Continued)

Name	R.A.[a] (J2000)	Decl.	$m-M$[b] (mag)	Method[c]	K[d] (2MASS)	σ[e] (km s^{-1})	$M(\mathrm{BH})_K$[f] ($10^8\ M_\odot$)	$M(\mathrm{BH})_\sigma$[g] ($10^8\ M_\odot$)	Notes[h]
NGC 7562	23:15:57	+06:41:14	33.8	SBF	8.32	256	9.03	5.51	
NGC 7600	23:18:53	−07:34:49	33.4	CV	8.91	210	3.56	2.10	
NGC 7618	23:19:47	+42:51:09	34.3	CV	9.04	298	7.35	11.53	
NGC 7626	23:20:42	+08:13:01	33.7	SBF	8.03	271	10.66	7.27	
NGC 7711	23:35:39	+15:18:07	33.8	CV	8.91	180	4.93	0.99	
NGC 7743	23:44:21	+09:56:02	31.6	SBF	8.42	84	0.97	0.02	
NGC 7785	23:55:19	+05:54:57	33.8	D_n–σ	8.45	255	7.98	5.41	

Notes.
[a] J2000 coordinates, from the NASA/IPAC Extragalactic Database (NED, http://ned.ipac.caltech.edu).
[b] Distance modulus estimate, using the method identified in Column 5, as listed in the NASA/IPAC Extragalactic Database (NED, http://ned.ipac.caltech.edu).
[c] Method used in determining the distance modulus. For uniformity, preference was given to surface brightness fluctuation (SBF) distances, followed by Type Ia Supernova (SNIa) distances, distances based on the Tully–Fisher (TF) relation and D_n–σ relations, and redshift distances (CV). The latter are calculated from the recessional velocity (as listed in NED) divided by $H_0 = 72$ km s^{-1} Mpc^{-1} (Freedman et al. 2000). Specific references can be found in NED.
[d] The total K-band magnitude derived from fit extrapolation, as listed in the 2MASS database (http://irsa.ipac.caltech.edu/cgi-bin/Gator/nph-dd, Jarrett 2000).
[e] Average value of the stellar velocity dispersion, computed from all available sources following the precepts of Prugniel & Simien (1996), as listed in the HyperLeda database (http://leda.univ-lyon1.fr/).
[f] Black hole mass estimated from the K-band magnitude listed in Column 6, following Equation (7) of Vika et al. (2012).
[g] Black hole mass estimated from the stellar velocity dispersion listed in Column 7, following Equation (20) of Ferrarese & Ford (2005).
[h] Black hole masses based on dynamical models applied to spatially resolved kinematics are listed when available.
References. (1) Sarzi et al. 2001; (2) van der Marel & van den Bosch 1998; (3) Gebhardt et al. 2007; (4) Barth et al. 2001; (5) Gultekin et al. 2009; (6) Ferrarese & Ford 1999.

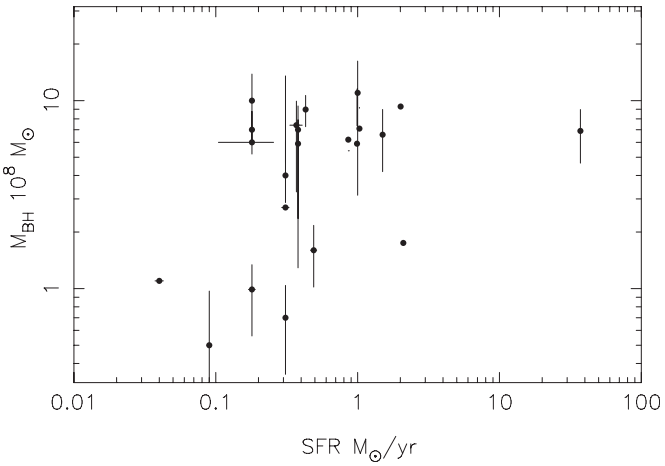

Figure 9. SFR and black hole mass from Tables 2 and 4.

Photoionization by hard radiation from close to the BH could also strengthen Brγ over the value due to star formation.

5. CONCLUSIONS

Some 20% of ellipticals in the Brown et al. (2011) sample have emission-line nuclei, which will be followed up with IFU spectrographs on AO-equipped telescopes. The complete sample may have a somewhat lower emission fraction, as galaxies with optical emission lines (where this was known) tended to be observed first in order to provide immediate targets for IFU observing. Emission-line nuclei are accompanied by more powerful radio sources at a given galaxy mass.

The SFR in these nuclei has a median value of 0.4 $M_\odot$ yr^{-1} and must be intermittent to attain the median BH mass of $5 \times 10^8\ M_\odot$ of these galaxies.

Thanks go to Eilat Glickman for sharing her observing expertise at the Palomar 200 inch telescope and her copy of the Triplespec Spextool IDL program. This paper has also made use of IRAF, which is distributed by NOAO. NOAO is operated by AURA under a cooperative agreement with NSF. The Caltech-Swinburne Collaborative Agreement allows the first author access to the Hale and Keck telescopes. Survey astronomy is supported by the Australian Research Council through CAASTRO.[14] The Centre for All-sky Astrophysics is an Australian Research Council Centre of Excellence, funded by grant CE11001020. G.C. acknowledges support from STFC grants ST/H002456/1 and ST/I003673/1. M.B. acknowledges the support from the Australian Research Council via Future Fellowship FT100100280 and Discovery Project DP110102174. We thank an anonymous referee for comments which improved the paper.

REFERENCES

Antonucci, R., Hickson, P., Miller, J. S., & Olszewski, E. W. 1987, AJ, 93, 785
Balzano, V. 1983, ApJ, 268, 602
Barth, A., Greene, J., & Ho, L. 2005, ApJ, 619, L151

[14] www.caastro.org

Barth, A., Sarzi, M., Rix, H.-W., et al. 2001, ApJ, 555, 685
Best, P., Kaiser, C., Heckman, T., & Kauffmann, G. 2006, MNRAS, 368, L67
Bower, R., Benson, A., Malbon, R., et al. 2006, MNRAS, 370, 645
Brown, M. J. I., Jannuzi, B., Floyd, D., & Mould, J. 2011, ApJ, 731, 41
Cesetti, M., Ivanov, V. D., Morelli, L., et al. 2009, A&A, 497, 41
Cushing, M., Vacca, W., & Rayner, J. 2004, PASP, 116, 362
Fabbiano, G., Gioia, I. M., & Trinchieri, G. 1989, ApJ, 347, 127
Ferrarese, L., & Ford, H. F. 1999, ApJ, 515, 583
Ferrarese, L., & Ford, H. F. 2005, Space Sci. Rev., 116, 523
Ferrarese, L., & Merritt, D. 2000, ApJ, 539, L9
Freedman, W. L., Madore, B. F., Gibson, B. K., et al. 2000, ApJ, 553, 47
Gebhardt, K., Bender, R., Bower, G., et al. 2000, ApJ, 539, L13
Gebhardt, K., Lauer, T. R., Pinkney, J., et al. 2007, ApJ, 671, 1321
Graham, A. 2007, MNRAS, 379, 711
Granato, G. L., De Zotti, G., Silva, L., Bressan, A., & Danese, L. 2004, ApJ, 600, 580
Greene, J. E., & Ho, L. C. 2006, ApJ, 641, L21
Greene, J. E., & Ho, L. C. 2007, ApJ, 667, 131
Gultekin, K., Richstone, D. O., Gebhardt, K., et al. 2009, ApJ, 695, 1577
Hardcastle, M., Evans, D., & Croston, J. 2006, MNRAS, 376, 1849
Ho, L. 1999, ApJ, 510, 631
Ho, L. 2008, ARA&A, 46, 475
Hopkins, P. F., & Hernquist, L. 2006, ApJS, 166, 1
Hopkins, P. F., Hernquist, L., Cox, T. J., & Kereš, D. 2008, ApJS, 175, 356
Jahnke, K., & Maccio, A. 2010, ApJ, 734, 92
Jarrett, T. H. 2000, PASP, 112, 1008
Kennicutt, R. 1998, ARA&A, 36, 189
Kormendy, J. 1993, in The Nearest Active Galaxies, ed. J. Beckman, L. Colina, & H. Netzer (Madrid: Consejo Superior de Investigaciones Cientificas), 197
Kormendy, J. 2004, Coevolution of Black Holes and Galaxies (Carnegie Observatories Astrophysics Series, Vol. 1; Cambridge: Cambridge Univ. Press)
Kormendy, J., & Richstone, D. O. 1995, ARA&A, 33, 581
Lynden-Bell, D., & Rees, M. 1971, MNRAS, 152, 461
Magorrian, J., Tremaine, S., Richstone, D., et al. 1998, AJ, 115, 2285
Mayes, A. J., Evans, A., & Pearce, G. 1985, A&A, 143, 327
Murakami, H., Baba, H., Barthel, P., et al. 2007, PASJ, 59, 369
Prugniel, P., & Simien, F. 1996, A&A, 309, 749
Riffel, R., Rodrguez-Ardila, A., & Pastoriza, M. G. 2006, A&A, 457, 61
Sadler, E. M., Jenkins, C. R., & Kotanyi, C. G. 1989, MNRAS, 240, 591
Slee, O. B., Sadler, E. M., Reynolds, J. E., & Ekers, R. D. 1994, MNRAS, 269, 928
Sarzi, M., Rix, H.-W., Shields, J. C., et al. 2001, ApJ, 550, 65
Springel, V., Di Matteo, T., & Hernquist, L. 2005, MNRAS, 361, 776
van der Marel, R. P., & van den Bosch, F. C. 1998, AJ, 116, 2220
Veron-Cetty, M., & Veron, P. 2006, A&A, 455, 773
Vika, M., Driver, S. P., Cameron, E., Kelvin, L., & Robotham, A. 2012, MNRAS, 419, 2264